

A multilayer multiconfiguration time-dependent Hartree study of the nonequilibrium Anderson impurity model at zero temperature

Haobin Wang

*Department of Chemistry, University of Colorado, Denver, CO 80217, USA and
Beijing Computational Science Research Center,
No.10 East Xibeiwang Road, Haidian District, Beijing 100193, China*

Michael Thoss

*Institute of Physics, University of Freiburg,
Hermann-Herder-Str. 3, D-79104 Freiburg, Germany*

(Dated: June 5, 2021)

Abstract

Quantum transport is studied for the nonequilibrium Anderson impurity model at zero temperature employing the multilayer multiconfiguration time-dependent Hartree theory within the second quantization representation (ML-MCTDH-SQR) of Fock space. To address both linear and nonlinear conductance in the Kondo regime, two new techniques of the ML-MCTDH-SQR simulation methodology are introduced: (i) the use of correlated initial states, which is achieved by imaginary time propagation of the overall Hamiltonian at zero voltage and (ii) the adoption of the logarithmic discretization of the electronic continuum. Employing the improved methodology, the signature of the Kondo effect is analyzed.

I. INTRODUCTION

Nonequilibrium quantum transport in molecular junctions or through quantum dots has received much attention recently, both as platform to study fundamental aspects of a nanoscale many-body quantum system out of equilibrium and due to potential applications in future devices.¹⁻¹⁰ Experimental observations of interesting transport phenomena, such as, e.g., Coulomb blockade,^{11,12} Kondo effect,¹³⁻¹⁷ negative differential resistance,¹⁸⁻²⁰ switching and hysteresis,²¹⁻²³ have inspired extensive theoretical developments. One class of theoretical methods is based on concepts such as perturbation theory, factorization ansatzes and/or effective single-particle approaches to tackle the complex many-body problem in an approximate way. Examples in the context of transport in molecular junctions include scattering theory,²⁴⁻³¹ nonequilibrium Green's function (NEGF) approaches,³²⁻⁴⁰ and master equation methods.^{33,41-53} The strength of these approaches is that they offer important physical insights into the problems of interest at low to moderate numerical effort. They are also often relatively easy to implement. Their limitation, on the other hand, is the lack of estimate or control of errors, such that it is often difficult to assess the accuracy of the theoretical predictions.

Thus, the development of another class of methods, which can be systematically converged, i.e. numerically exact methods, is essential to reliably address the difficult issues in nonequilibrium transport, in particular in the strong coupling regime. These methods include the numerical path integral approach,⁵⁴⁻⁵⁶ real-time quantum Monte Carlo simulations,⁵⁷⁻⁵⁹ the numerical renormalization group approach,⁶⁰ the time-dependent density matrix renormalization group approach,⁶¹ the hierarchical equations of motion method,⁶²⁻⁶⁷ a combination of reduced density matrix techniques and impurity solvers,^{68,69} and the multilayer multiconfiguration time-dependent Hartree (ML-MCTDH) theory in second quantization representation (SQR) developed by us.⁷⁰

In previous work, we have applied the ML-MCTDH-SQR method to several models of nonequilibrium quantum transport, including the vibrationally-coupled electron transport model, the Anderson impurity model, and their combination.^{69,71-73} Our simulations have illustrated important physical effects such as bistability, Coulomb and phonon blockade. Furthermore, employing a transformation of the Hamiltonian to an appropriate scattering states representation, we have demonstrated the role of quantum correlation in vibrationally-

coupled electron transport,⁷⁴ which is particularly important in the off-resonant transport regime dominated by cotunneling processes, where approximate approaches such as NEGF or Hartree-Fock predict an incorrectly large current.

In this paper, we employ the ML-MCTDH-SQR method to study the nonequilibrium Anderson impurity model at zero temperature. In this regime, the Anderson impurity model is known to exhibit Kondo effect.^{13,75,76} To facilitate the simulation of transport in this regime, we introduce two modifications to our existing approach. The first is the use of a correlated initial state, obtained by imaginary time propagation of the full Hamiltonian, to reduce transient peaks in the time-dependent current. The second is the use of Wilson's logarithmic discretization of the electronic continuum,⁷⁷ used extensively in the numerical renormalization group type of methods, to access the electronic states near the Fermi level of the electrodes. These two methodology adaptations allow us to address new physical regimes that are useful to study the effect of both linear and nonlinear conductance.

The remaining part of the paper is organized as follows. Sections II-IV outline the physical model, the discretization of the electronic continuum, the generation of the a correlated initial state, and the ML-MCTDH-SQR theory, respectively. Section V presents results of numerical simulations for a variety of parameter regimes as well as an analysis of the transport mechanisms. Section VI concludes with a summary.

II. MODEL AND OBSERVABLES OF INTEREST

In this paper we consider the single level Anderson impurity model⁷⁸ that has been investigated in great detail both in equilibrium and nonequilibrium.^{75,79} It exhibits interesting transport phenomena such as Coulomb blockade and Kondo effect. The model comprises one spatial electronic state localized at the molecular bridge or the quantum dot (in the following referred to as bridge state), which can be occupied with two electrons of different spin polarization and two electronic continua describing the electrodes (leads). The Hamiltonian reads

$$\begin{aligned} \hat{H} = & \sum_{\sigma} E_d \hat{n}_{d,\sigma} + U_d \hat{n}_{d,\uparrow} \hat{n}_{d,\downarrow} + \sum_{k_L,\sigma} E_{k_L} \hat{n}_{k_L,\sigma} + \sum_{k_R,\sigma} E_{k_R} \hat{n}_{k_R,\sigma} \\ & + \sum_{k_L,\sigma} V_{dk_L} (\hat{d}_{\sigma}^{\dagger} \hat{c}_{k_L,\sigma} + \hat{c}_{k_L,\sigma}^{\dagger} \hat{d}_{\sigma}) + \sum_{k_R,\sigma} V_{dk_R} (\hat{d}_{\sigma}^{\dagger} \hat{c}_{k_R,\sigma} + \hat{c}_{k_R,\sigma}^{\dagger} \hat{d}_{\sigma}). \end{aligned} \quad (2.1)$$

In the above expression, $\hat{n} = \hat{d}^\dagger \hat{d}$ denotes the number operator, subscript “ d ” refers to the bridge state, “ k_L/k_R ” the states of the left/right metal leads, and “ $\sigma = \uparrow, \downarrow$ ” the two spin indices. Operators \hat{d}^\dagger/\hat{d} , $\hat{c}_{k_L}^+/\hat{c}_{k_L}$, $\hat{c}_{k_R}^+/\hat{c}_{k_R}$ are the fermionic creation/annihilation operators for the electronic states on the molecular bridge, the left and the right leads, respectively. The second term in Eq. (2.1) describes the on-site Coulomb repulsion of the electrons on the molecular bridge with electron-electron coupling strength U_d . The energies of the electronic states in the leads, E_{k_L} , E_{k_R} , as well as the molecule-lead coupling parameters V_{dk_L} , V_{dk_R} are assumed to be independent of the spin polarization and are defined through the energy-dependent level width functions

$$\Gamma_L(E) = 2\pi \sum_{k_L} |V_{dk_L}|^2 \delta(E - E_{k_L}), \quad \Gamma_R(E) = 2\pi \sum_{k_R} |V_{dk_R}|^2 \delta(E - E_{k_R}). \quad (2.2)$$

The energies and couplings in the above model can be obtained in various ways. One approach is to perform electronic structure calculations to extract the model parameters.⁸⁰ In this paper, we consider a model parameterization for the electronic states of the leads, where the lead spectral density is an approximation to a square band,

$$\Gamma(E) = \frac{\Gamma}{[1 + e^{(E-E_c)/\delta}][1 + e^{-(E+E_c)/\delta}]}. \quad (2.3)$$

In the limit $\delta \rightarrow 0$, $E = \pm E_c$ defines the band edge, with $\Gamma(E) = \Gamma$ in between. The width functions for the left and the right leads are obtained by shifting $\Gamma(E)$ relative to the chemical potentials of the corresponding leads

$$\Gamma_L(E) = \Gamma(E - \mu_L), \quad \Gamma_R(E) = \Gamma(E - \mu_R), \quad (2.4)$$

We consider a model of two identical leads, in which the chemical potentials are given by

$$\mu_{L/R} = E_f \pm V/2, \quad (2.5)$$

where V is the bias voltage and E_f the Fermi energy of the leads.

An observable X of interest for studying time-dependent transport can be expressed by the following time correlation function (in this paper we use atomic units where $\hbar = e = 1$)

$$X(t) = \frac{1}{\text{tr}[\hat{\rho}]} \text{tr} \left[\hat{\rho} e^{i\hat{H}t} \hat{X} e^{-i\hat{H}t} \right]. \quad (2.6)$$

For example, for a given bias voltage the time-dependent currents for the left and right leads are given by

$$I_L(t) = -\frac{dN_L(t)}{dt} = -\frac{1}{\text{tr}[\hat{\rho}]} \text{tr} \left\{ \hat{\rho} e^{i\hat{H}t} i[\hat{H}, \hat{N}_L] e^{-i\hat{H}t} \right\}, \quad (2.7a)$$

$$I_R(t) = \frac{dN_R(t)}{dt} = \frac{1}{\text{tr}[\hat{\rho}]} \text{tr} \left\{ \hat{\rho} e^{i\hat{H}t} i[\hat{H}, \hat{N}_R] e^{-i\hat{H}t} \right\}, \quad (2.7b)$$

where $N_{L/R}(t)$ denotes the time-dependent charge in each lead

$$N_\zeta(t) = \frac{1}{\text{tr}[\hat{\rho}]} \text{tr}[\hat{\rho} e^{i\hat{H}t} \hat{N}_\zeta e^{-i\hat{H}t}], \quad \zeta = L, R, \quad (2.8)$$

and $\hat{N}_\zeta = \sum_{k_\zeta, \sigma} \hat{n}_{k_\zeta, \sigma}$ is the occupation number operator for the electrons in each lead ($\zeta = L, R$).

Other observables are also important for studying time-dependent quantum transport. Since the ML-MCTDH approach provides the wave function for the entire system, any properties can be obtained almost free of additional cost. For example, the electronic population of the bridge state with a particular spin σ is given by

$$n_{d, \sigma}(t) = \frac{1}{\text{tr}[\hat{\rho}]} \text{tr}[\hat{\rho} e^{i\hat{H}t} \hat{n}_{d, \zeta} e^{-i\hat{H}t}], \quad (2.9)$$

which can be used to analyze the nonequilibrium transport mechanisms.

III. DETAILS OF THE CALCULATION

In this section we discuss several important details of the calculation. Most of them are not only essential to the ML-MCTDH-SQR simulation but are also applicable to other approaches or have important physical relevance.

A. The Initial Condition

In the time correlation functions introduced in the previous section, $\hat{\rho}$ denotes the initial density matrix. It is usually written in a factorized form (but see below for a different choice), i.e., it is modeled by a grand-canonical ensemble for each lead and a particular occupation of the bridge state,

$$\hat{\rho}_e = \hat{\rho}_d^0 \exp \left[-\beta(\hat{H}_e^0 - \mu_L \hat{N}_L - \mu_R \hat{N}_R) \right], \quad (3.1a)$$

$$\hat{H}_e^0 = \sum_{k_L, \sigma} E_{k_L} \hat{n}_{k_L, \sigma} + \sum_{k_R, \sigma} E_{k_R} \hat{n}_{k_R, \sigma}. \quad (3.1b)$$

Thereby, $\hat{\rho}_d^0$ is the initial reduced density matrix for the molecular bridge, which can be chosen as a pure state representing either occupied or empty bridge states. Other initial

states may also be used. For example, one may use a fully correlated initial state,

$$\hat{\rho} = \exp \left[-\beta(\hat{H} - \mu_L \hat{N}_L - \mu_R \hat{N}_R) \right], \quad (3.2)$$

employing the imaginary time ML-MCTDH propagation, which is similar to what we have proposed previously for a canonical ensemble.⁸¹ This is particularly advantageous for studying the steady-state current at strong coupling regimes where a factorized initial state results in strong transient effect in the current.

B. Discretization of the Nuclear and Electronic Continua

Since ML-MCTDH simulations employ wave functions explicitly for all degrees of freedom, the continua of the two electrodes need to be discretized. This is similar to a numerical integration, and there are various ways to achieve the goal of an efficient discretization. Formally, the electronic continuum for the two leads can be discretized by choosing a density of states $\rho_e(E)$ such that⁸²⁻⁸⁴

$$\int_{-E_M}^{E_k} dE \rho_e(E) = k, \quad |V_{dk}|^2 = \frac{\Gamma(E_k)}{2\pi\rho_e(E_k)}, \quad k = 1, \dots, N_e, \quad (3.3)$$

where N_e is the number of electronic states (for a single spin/single lead) in the simulation. This is essentially a quadrature representation of an integral that involves $\Gamma(E)$. Very often a constant $\rho_e(E)$, i.e., an equidistant discretization of the whole band interval, works best for representing the electronic continuum. This corresponds to a sinc-function quadrature which is known to be effective for handling oscillatory integrands. However, for some problems it is well-known (and we will show this numerically in this paper) that Wilson's logarithmic discretization scheme⁷⁷ is more efficient to focus on the electronic states near the Fermi level. For states above the Fermi level, this discretization scheme gives

$$\frac{E_k - E_f}{E_M - E_k} = \Lambda^{M-k}, \quad (3.4)$$

where $\Lambda \rightarrow 1^+$, $M = N_e/2$, and E_M is the energy of the band edge. For a symmetric band, the states below the Fermi level are obtained by symmetry, otherwise the above relation is simply modified via $E \rightarrow -E$.

From a general perspective, Wilson's logarithmic discretization employs a relation similar to (3.3) based on a particular density of states

$$\int_{E_k}^{E_M} dE \rho_e(E) = M - k, \quad (3.5)$$

It is easy to verify that the density of states satisfying Eq. (3.4) is given by

$$\rho_e(E) = \frac{1}{(E - E_f)\ln\Lambda}. \quad (3.6)$$

In many applications, one does not take E_k in Eq. (3.4) but rather an average energy \bar{E}_k ,

$$\bar{E}_k = \frac{\int^k dE \rho_e(E) E}{\int^k dE \rho_e(E)}, \quad (3.7a)$$

where

$$\int^k dE \equiv \int_{E_{k-1}}^{E_k} dE. \quad (3.7b)$$

Moreover, the density of states $\rho_e(E)$ does not need to be a continuous function in the whole interval as Eq. (3.6). Instead, in many NRG applications $\rho_e(E)$ is chosen to be piecewise continuous in each of the $[E_{k-1}, E_k]$ interval, where E_k is given in (3.4). Within each such interval one is free to choose a particular $\rho_e(E)$ such that

$$\int^k dE \rho_e(E) = 1. \quad (3.8)$$

For example, one may require that $\rho_e(E) \propto \Gamma(E)$ in each interval as done in many NRG applications. Our investigation shows that these different variants make negligible difference in our applications when the number of discrete states is large enough (e.g., > 100).

C. Regularization of the Current

The transient behavior of the single-lead currents $I_R(t)$ and $I_L(t)$ defined in Eq. (2.7) is usually different. However, the long-time limits of $I_R(t)$ and $I_L(t)$, which define the steady-state current, are the same. It is found that the average current

$$I(t) = \frac{1}{2}[I_R(t) + I_L(t)], \quad (3.9)$$

provides better numerical convergence properties by minimizing the transient characteristic, and thus will be used in most calculations.

Since the electronic continuum is represented by a finite number of states, recurrences will eventually occur at longer times. This time scale depends on the number of states used in the simulation. The situation is thus similar to that of a quantum reactive scattering calculation in the presence of a scattering continuum, where, with a finite number of basis functions, an

appropriate absorbing boundary condition is added to mimic the correct outgoing Green's function.^{85–88} Employing the same strategy for the present problem, the regularized electric current is given by

$$I^{\text{reg}} = \lim_{\eta \rightarrow 0^+} \int_0^\infty dt \frac{dI(t)}{dt} e^{-\eta t}. \quad (3.10)$$

The regularization parameter η is similar (though not identical) to the formal convergence parameter in the definition of the Green's function in terms of the time evolution operator

$$G(E^+) = \lim_{\eta \rightarrow 0^+} (-i) \int_0^\infty dt e^{i(E+i\eta-H)t}. \quad (3.11)$$

In numerical calculations, the parameter η has to be large enough to accelerate the convergence but still sufficiently small in order not to affect the correct result. While in the reactive scattering calculation η is often chosen to be coordinate dependent, here η is chosen to be time dependent

$$\eta(t) = \begin{cases} 0 & (t < \tau) \\ \eta_0 \cdot (t - \tau)/t & (t > \tau). \end{cases} \quad (3.12)$$

Here η_0 is a damping constant, τ is a cutoff time beyond which a steady state charge flow is approximately reached. As the number of electronic states increases, one may choose a weaker damping strength η_0 and/or longer cutoff time τ . The former approaches zero and the latter approaches infinity for an infinite number of states.

IV. THE MULTILAYER MULTICONFIGURATION TIME-DEPENDENT HARTREE THEORY IN SECOND QUANTIZATION REPRESENTATION

To describe many-body quantum dynamics in an efficient way, we employ the multilayer multiconfiguration time-dependent Hartree (ML-MCTDH) theory in second quantization representation (SQR).⁸⁹ The ML-MCTDH theory^{84,90} is a rigorous variational method to propagate wave packets in complex systems with many degrees of freedom. In this approach the wave function is represented by a recursive, layered expansion,

$$|\Psi(t)\rangle = \sum_{j_1} \sum_{j_2} \dots \sum_{j_p} A_{j_1 j_2 \dots j_p}(t) \prod_{\kappa=1}^p |\varphi_{j_\kappa}^{(\kappa)}(t)\rangle, \quad (4.1a)$$

$$|\varphi_{j_\kappa}^{(\kappa)}(t)\rangle = \sum_{i_1} \sum_{i_2} \dots \sum_{i_{Q(\kappa)}} B_{i_1 i_2 \dots i_{Q(\kappa)}}^{\kappa, j_\kappa}(t) \prod_{q=1}^{Q(\kappa)} |v_{i_q}^{(\kappa, q)}(t)\rangle, \quad (4.1b)$$

$$|v_{i_q}^{(\kappa,q)}(t)\rangle = \sum_{\alpha_1} \sum_{\alpha_2} \dots \sum_{\alpha_{M(\kappa,q)}} C_{\alpha_1 \alpha_2 \dots \alpha_{M(\kappa,q)}}^{\kappa,q,i_q}(t) \prod_{\gamma=1}^{M(\kappa,q)} |\xi_{\alpha_\gamma}^{\kappa,q,\gamma}(t)\rangle, \quad (4.1c)$$

where $A_{j_1 j_2 \dots j_p}(t)$, $B_{i_1 i_2 \dots i_{Q(\kappa)}}^{\kappa,j_\kappa}(t)$, $C_{\alpha_1 \alpha_2 \dots \alpha_{M(\kappa,q)}}^{\kappa,q,i_q}(t)$ and so on are the expansion coefficients for the first, second, third, ..., layers, respectively; $|\varphi_{j_\kappa}^{(\kappa)}(t)\rangle$, $|v_{i_q}^{(\kappa,q)}(t)\rangle$, $|\xi_{\alpha_\gamma}^{\kappa,q,\gamma}(t)\rangle$, ..., are the “single particle” functions (SPFs) for the first, second, third, ..., layers. In Eq. (4.1a), p denotes the number of single particle (SP) groups/subspaces for the first layer. Similarly, $Q(\kappa)$ in Eq. (4.1b) is the number of SP groups for the second layer that belongs to the κ th SP group in the first layer, i.e., there are a total of $\sum_{\kappa=1}^p Q(\kappa)$ second layer SP groups. Continuing along the multilayer hierarchy, $M(\kappa, q)$ in Eq. (4.1c) is the number of SP groups for the third layer that belongs to the q th SP group of the second layer and the κ th SP group of the first layer, resulting in a total of $\sum_{\kappa=1}^p \sum_{q=1}^{Q(\kappa)} M(\kappa, q)$ third layer SP groups.

ML-MCTDH is an effective tensor contraction scheme. Its mathematical form in (4.1) has been given various names such as the hierarchical low rank tensor format, the tree Tucker format, the tensor train format, and the sequential unfolding SVD.⁹⁰ The size of the system that the ML-MCTDH theory can treat increases with the number of layers in the expansion. In principle, such a recursive expansion can be carried out to an arbitrary number of layers. The multilayer hierarchy is terminated at a particular level by expanding the SPFs in the deepest layer in terms of time-independent configurations, each of which may still contain several Cartesian degrees of freedom. The variational parameters within the ML-MCTDH theoretical framework are dynamically optimized through the use of the Dirac-Frenkel variational principle⁹¹

$$\langle \delta \Psi(t) | i \frac{\partial}{\partial t} - \hat{H} | \Psi(t) \rangle = 0, \quad (4.2)$$

which results in a set of coupled, nonlinear differential equations for the expansion coefficients for all layers.^{70,84,89}

The development of the ML-MCTDH method was motivated by the original MCTDH method^{92–96} and extends its applicability to significantly larger systems.^{81,84,97–100} The theory has also been generalized to study heat transport in molecular junctions¹⁰¹ and to calculate thermal rate constants for condensed phase systems using the reactive flux correlation function formalism.^{100,102} The work of Manthe has introduced an even more adaptive formulation based on a layered correlation discrete variable representation (CDVR).^{103,104} ML-MCTDH

has also been implemented in the popular Heidelberg MCTDH program package.⁹⁶ Recently, the ML-MCTDH theory has been formulated within an interaction picture to remove artificial correlation.^{73,105}

Another hurdle to overcome for the study of electron transport processes is that the methodology has to be adapted to handle identical quantum particles, i.e., to incorporate the exchange symmetry explicitly. Within the (single-layer) MCTDH method, one may employ a properly symmetrized wave function in the first quantized framework, i.e., permanents in a bosonic case¹⁰⁶ or Slater determinants in a fermionic case.^{107–109} However, this wave function-based symmetrization is incompatible with the ML-MCTDH theory with more layers — there is no obvious analog of a multilayer Hartree configuration if permanents/determinants are used to represent the wave function. Therefore, we proposed a novel approach, the ML-MCTDH-SQR method,⁷⁰ that follows a fundamentally different route to tackle many-body quantum dynamics of indistinguishable particles — an operator-based method that employs the second quantization formalism of many-particle quantum theory. This differs from many previous methods where the second quantization formalism is only used as a convenient tool to derive intermediate expressions for the first quantized form. In the ML-MCTDH-SQR approach the variation is carried out entirely in the abstract Fock space using the occupation number representation. Therefore, the burden of handling symmetries of identical particles in a numerical variational calculation is shifted completely from wave functions to the algebraic properties of operators. For example, in the second quantized form the fermionic creation/annihilation operators fulfill the anti-commutation relations

$$\{\hat{a}_P, \hat{a}_Q^+\} \equiv \hat{a}_P \hat{a}_Q^+ + \hat{a}_Q^+ \hat{a}_P = \delta_{PQ}, \quad \{\hat{a}_P^+, \hat{a}_Q^+\} = \{\hat{a}_P, \hat{a}_Q\} = 0. \quad (4.3)$$

The symmetry of identical particles is thus realized by enforcing such algebraic properties of the operators. This can be accomplished by introducing a permutation sign operator associated with each fermionic creation/annihilation operator, which incorporates the sign changes of the remaining spin orbitals in all the SPFs whose subspaces are prior to it.⁷⁰

In the second quantized form, the wave function is represented in the abstract Fock space employing the occupation number basis. This is not plausible if one is only interested in a single configuration-based method, e.g., Hartree-Fock or Kohn-Sham density functional theory. However, it is advantageous when one aims at treating correlation effect in a numerically exact way via a multiconfigurational method, especially in the multilayer form.

Within the second quantization representation, any wave function can be easily expanded in the same multilayer form as that for systems of distinguishable particles. All the ML-MCTDH techniques can thus be adopted naturally. The symmetry of the wave function in the first quantized form is shifted to the operator algebra in the second quantized form. The key point is that, for both phenomenological models and more fundamental theories, there are only a limited number of combination of fundamental operators. For example, in electronic structure theory only one- and two-electron operators are present. This means that one never needs to handle all, redundant possibilities of operator combinations as offered by the determinant form in the first quantized framework. It is exactly this property that provides the flexibility of representing the wave functions in multilayer form and treat them accurately and efficiently within the ML-MCTDH theory.

It is noted that Manthe et al. have presented a variant of the ML-MCTDH-SQR approach using optimized time-dependent orbitals.¹¹⁰ Furthermore, the concept of the SQR has also been used recently within a single layer MCTDH implementation to study impurity models.¹¹¹

V. RESULTS AND DISCUSSION

In this section, we apply the ML-MCTDH methodology outlined above to the Anderson impurity model at zero temperature. In this regime, the Anderson impurity model is known to exhibit Kondo effect,^{13,75,76} which manifests itself in a many-body resonance of the conductance at the Fermi energy. We specifically consider the particle-hole symmetric regime with $E_d = -U_d/2$, where the Kondo resonance for the zero-bias conductance exhibits a maximal value of the conductance quantum G_0 .

Figure 1 shows the current as a function of time for a bias voltage of $V = 0.1$ V and different values of Coulomb repulsion $U_d = -2E_d$. After a transient regime the current saturates to a steady state plateau, the value of which decreases for larger U_d , in accordance with the energy level scheme.

For the voltage of $V = 0.1$ eV used in Figure 1, which is already outside the linear response regime, the current can be simulated directly as discussed above. For smaller voltages, as is necessary to access, e.g., the zero-bias conductance, the direct simulation of the current using the standard factorized initial density matrix and equal-spaced discretization

of the electronic continuum becomes numerically challenging. This can be attributed to two physical reasons. First, due to the large transient peaks in the time-dependent current, the noise to signal ratio for the steady state current becomes large. Second, to facilitate the current at very small bias voltage, states of the electrodes near the Fermi level become important. An equal-spaced discretization is in this case inefficient and the calculation would require many more states to converge.

The second issue is related to the particular physics in the Kondo regime and has been studied previously. To focus on the states near the Fermi level, the scheme pioneered by Wilson,⁷⁷ Eqs. (3.4)-(3.8), has proven to be very effective. It is widely used in numerical renormalization group (NRG) theory calculations, typically with a relatively large value of the parameter $\Lambda \sim 2$. Unlike in NRG, the ML-MCTDH simulation can easily treat more than 200 states per lead, which enables us to examine the limit $\Lambda \rightarrow 1^+$ in Eq. (3.4).

The use of Wilson's logarithmic discretization scheme, however, does not solve the first problem related to the factorized initial density matrix. In fact, it makes the situation even worse since the electronic states are no longer arranged as Fourier grids. As a result, the time-dependent current exhibits severe oscillations, which is demonstrated in Figure 2. This problem is also known in NRG, where a time-averaging scheme is often employed to smooth the long-time current.⁶⁰ For this purpose one may also apply the regularization scheme described earlier in this paper.

A more robust way towards the same goal is to employ a correlated initial density matrix, Eq. (3.2). At a finite temperature this is achieved by combining imaginary time ML-MCTDH propagation with a Monte Carlo importance sampling scheme.⁸¹ For the case of zero temperature, it is done as an imaginary time ML-MCTDH propagation (relaxation) with a sufficiently large imaginary time $\beta = 1/k_B T$. As shown in Figure 2, the use of a correlated initial density matrix improves the situation significantly. The current fluctuates only within a few percent relative deviation, which does not show up in the scale of the plot. Within the numerical resolution, $T = 2.5K$ for the imaginary time propagation is satisfactory for this example. Nevertheless, this is a convergence parameter and needs to be tested. For the parameter regime discussed in this paper convergence is achieved within the range of 0.5 - 10 K.

Within Wilson's logarithmic discretization scheme, varying the parameter Λ in Eq. (3.4) has some influence on the value of the calculated current, as shown in Figure 3. For a fixed

number of discrete states, a too small Λ results in an insufficient number of states near the Fermi level and thus too small a current. On the other hand, a larger Λ results in a larger amplitude of oscillation in the current. Convergence is achieved by reducing Λ while increasing the number of discrete states at the same time. In Figure 3, most steady-state currents agree well with each other except for the smallest and the largest Λ .

With these methodological improvements, it is possible to examine the steady-state current in the Kondo regime even for very small voltages. As an example, Figure 4 shows the time-dependent current for a bias voltage of 0.001V. For not too large Coulomb repulsion U_d , the steady-state current (and hence the conductance) is the same for different values of E_d as long as $E_d = -U_d/2$ is maintained. For larger values, e.g. $E_d = -U_d/2 = -0.16$ eV, the conductance is however no longer in the linear regime and therefore attains a smaller value. Simulations for even smaller bias voltage $V = 0.0001V$ show that $E_d = -U_d/2 = -0.16$ eV has the same steady-state current as for the other values of E_d and, thus, is in the linear conductance regime.

Figure 5 shows the conductance as a function of the bias voltage for different Coulomb repulsion strengths, where the relation $E_d = -U_d/2$ is maintained. The transition from the broad single-particle resonance for the noninteracting model ($U_d = 0$) to the many-body Kondo resonance is seen. As the electron-electron coupling increases, the width of the Kondo resonance becomes narrower, in qualitative accordance with approximate analytical theories.¹¹²

VI. CONCLUDING REMARKS

In this paper, we have employed the ML-MCTDH-SQR method to study correlated electron transport in the Anderson-impurity model at zero temperature. Extending our previous work,^{70,72} we have implemented Wilson's logarithmic discretization scheme for the electronic continuum, such that states near the Fermi level are taken into account with a higher weight, and the imaginary time propagation to obtain a correlated initial wave function. These improvements of the methodology allow us to address both linear and nonlinear conductance and to study more difficult physical regimes.

We have specifically focused on nonequilibrium transport at zero temperature. In this regime, the Anderson impurity model exhibits Kondo effect. Our calculations reveal the

Kondo resonance and show the dependence of the Kondo peak line shape on the strength of the Coulomb repulsion. The ability of obtaining this limit demonstrates that ML-MCTDH-SQR is a useful theory for studying nonequilibrium correlated quantum transport.

Acknowledgments

This paper is dedicated to Hans-Dieter Meyer on the occasion of his 70th birthday. The work has been supported by the National Science Foundation CHE-1500285 (HW) and the German Science Foundation (DFG) (MT) through SFB 953 and a research grant, and used resources of the National Energy Research Scientific Computing Center (NERSC), which is supported by the Office of Science of the U.S. Department of Energy under Contract No. DE-AC02-05CH11231.

-
- ¹ M. Reed, C. Zhou, C. Muller, T. Burgin, and J. Tour, *Science* **278**, 252 (1997).
- ² C. Joachim, J. Gimzewski, and A. Aviram, *Nature (London)* **408**, 541 (2000).
- ³ A. Nitzan, *Annu. Rev. Phys. Chem.* **52**, 681 (2001).
- ⁴ A. Nitzan and M. A. Ratner, *Science* **300**, 1384 (2003).
- ⁵ G. Cuniberti, G. Fagas, and K. Richter, *Introducing Molecular Electronics* (Springer, Heidelberg, 2005).
- ⁶ Y. Selzer and D. L. Allara, *Annu. Rev. Phys. Chem.* **57**, 593 (2006).
- ⁷ L. Venkataraman, J. E. Klare, C. Nuckolls, M. S. Hybertsen, and M. L. Steigerwald, *Nature* **442**, 904 (2006).
- ⁸ F. Chen, J. Hihath, Z. Huang, X. Li, and N. Tao, *Annu. Rev. Phys. Chem.* **58**, 535 (2007).
- ⁹ M. Galperin, M. A. Ratner, A. Nitzan, and A. Troisi, *Science* **319**, 1056 (2008).
- ¹⁰ J. Cuevas and E. Scheer, *Molecular Electronics: An Introduction to Theory and Experiment* (World Scientific, Singapore, 2010).
- ¹¹ J. Park, A. Pasupathy, J. Goldsmith, C. Chang, Y. Yaish, J. Petta, M. Rinkoski, J. Sethna, H. Abruna, P. McEuen, and D. Ralph, *Nature (London)* **417**, 722 (2002).
- ¹² H. B. Heersche, Z. de Groot, J. A. Folk, H. S. J. van der Zant, C. Romeike, M. R. Wegewijs, L. Zobbi, D. Barreca, E. Tondello, and A. Cornia, *Phys. Rev. Lett.* **96**, 206801 (2006).
- ¹³ W. Liang, M. Shores, M. Bockrath, J. Long, and H. Park, *Nature (London)* **417**, 725 (2002).
- ¹⁴ N. Roch, S. Florens, T. A. Costi, W. Wernsdorfer, and F. Balestro, *Phys. Rev. Lett.* **103**, 197202 (2009).
- ¹⁵ J. J. Parks, A. R. Champagne, T. A. Costi, W. W. Shum, A. N. Pasupathy, E. Neuscamman, S. Flores-Torres, P. S. Cornaglia, A. A. Aligia, C. A. Balseiro, G. K.-L. Chan, H. D. Abruña, *et al.*, *Science* **328**, 1370 (2010).
- ¹⁶ V. Meded, A. Bagrets, K. Fink, R. Chandrasekar, M. Ruben, F. Evers, A. Bernard-Mantel, J. S. Seldenthuis, A. Beukman, and H. S. J. van der Zant, *Phys. Rev. B* **83**, 245415 (2011).
- ¹⁷ T. Esat, B. Lechtenberg, T. Deilmann, C. Wagner, P. Krüger, R. Temirov, M. Rohlfing, F. Anders, and F. Tautz, *Nat. Phys.* **12**, 867 (2016).
- ¹⁸ J. Chen, M. Reed, A. Rawlett, and J. Tour, *Science* **286**, 1550 (1999).
- ¹⁹ J. Gaudioso, L. J. Lauhon, and W. Ho, *Phys. Rev. Lett.* **85**, 1918 (2000).

- ²⁰ E. A. Osorio, M. Ruben, J. S. Seldenthuis, J. M. Lehn, and H. S. J. van der Zant, *Small* **6**, 174 (2010).
- ²¹ A. Blum, J. Kushmerick, D. Long, C. Patterson, J. Jang, J. Henderson, Y. Yao, J. Tour, R. Shashidhar, and B. Ratna, *Nat. Mater.* **4**, 167 (2005).
- ²² E. Lörtscher, J. W. Ciszek, J. Tour, and H. Riel, *Small* **2**, 973 (2006).
- ²³ B.-Y. Choi, S.-J. Kahng, S. Kim, H. Kim, H. Kim, Y. Song, J. Ihm, and Y. Kuk, *Phys. Rev. Lett.* **96**, 156106 (2006).
- ²⁴ J. Bonca and S. Trugmann, *Phys. Rev. Lett.* **75**, 2566 (1995).
- ²⁵ H. Ness, S. Shevlin, and A. Fisher, *Phys. Rev. B* **63**, 125422 (2001).
- ²⁶ M. Cizek, M. Thoss, and W. Domcke, *Phys. Rev. B* **70**, 125406 (2004).
- ²⁷ M. Cizek, M. Thoss, and W. Domcke, *Czech. J. Phys.* **55**, 189 (2005).
- ²⁸ M. Caspary-Toroker and U. Peskin, *J. Chem. Phys.* **127**, 154706 (2007).
- ²⁹ C. Benesch, M. Cizek, J. Klimes, I. Kondov, M. Thoss, and W. Domcke, *J. Phys. Chem. C* **112**, 9880 (2008).
- ³⁰ N. A. Zimbovskaya and M. M. Kuklja, *J. Chem. Phys.* **131**, 114703 (2009).
- ³¹ R. Jorn and T. Seidemann, *J. Chem. Phys.* **131**, 244114 (2009).
- ³² K. Flensberg, *Phys. Rev. B* **68**, 205323 (2003).
- ³³ A. Mitra, I. Aleiner, and A. J. Millis, *Phys. Rev. B* **69**, 245302 (2004).
- ³⁴ M. Galperin, M. Ratner, and A. Nitzan, *Phys. Rev. B* **73**, 045314 (2006).
- ³⁵ D. A. Ryndyk, M. Hartung, and G. Cuniberti, *Phys. Rev. B* **73**, 045420 (2006).
- ³⁶ T. Frederiksen, M. Paulsson, M. Brandbyge, and A. Jauho, *Phys. Rev. B* **75**, 205413 (2007).
- ³⁷ M. Tahir and A. MacKinnon, *Phys. Rev. B* **77**, 224305 (2008).
- ³⁸ R. Härtle, C. Benesch, and M. Thoss, *Phys. Rev. B* **77**, 205314 (2008).
- ³⁹ J. P. Bergfield and C. A. Stafford, *Phys. Rev. B* **79**, 245125 (2009).
- ⁴⁰ R. Härtle, C. Benesch, and M. Thoss, *Phys. Rev. Lett.* **102**, 146801 (2009).
- ⁴¹ V. May, *Phys. Rev. B* **66**, 245411 (2002).
- ⁴² J. Lehmann, S. Kohler, V. May, and P. Hänggi, *J. Chem. Phys.* **121**, 2278 (2004).
- ⁴³ J. N. Pedersen and A. Wacker, *Phys. Rev. B* **72**, 195330 (2005).
- ⁴⁴ U. Harbola, M. Esposito, and S. Mukamel, *Phys. Rev. B* **74**, 235309 (2006).
- ⁴⁵ A. Zazunov, D. Feinberg, and T. Martin, *Phys. Rev. B* **73**, 115405 (2006).
- ⁴⁶ L. Siddiqui, A. W. Ghosh, and S. Datta, *Phys. Rev. B* **76**, 085433 (2007).

- 47 C. Timm, Phys. Rev. B **77**, 195416 (2008).
- 48 V. May and O. Kühn, Phys. Rev. B **77**, 115439 (2008).
- 49 V. May and O. Kühn, Phys. Rev. B **77**, 115440 (2008).
- 50 M. Leijnse and M. R. Wegewijs, Phys. Rev. B **78**, 235424 (2008).
- 51 M. Esposito and M. Galperin, Phys. Rev. B **79**, 205303 (2009).
- 52 R. Volkovich, R. Härtle, M. Thoss, and U. Peskin, Phys. Chem. Chem. Phys. **13**, 14333 (2011).
- 53 R. Härtle and M. Thoss, Phys. Rev. B **83**, 115414 (2011).
- 54 L. Mühlbacher and E. Rabani, Phys. Rev. Lett. **100**, 176403 (2008).
- 55 S. Weiss, J. Eckel, M. Thorwart, and R. Egger, Phys. Rev. B **77**, 195316 (2008).
- 56 D. Segal, A. J. Millis, and D. Reichman, Phys. Rev. B **82**, 205323 (2010).
- 57 P. Werner, T. Oka, and A. J. Millis, Phys. Rev. B **79**, 035320 (2009).
- 58 M. Schiro and M. Fabrizio, Phys. Rev. B **79**, 153302 (2009).
- 59 G. Cohen, E. Gull, D. Reichman, and A. Millis, Phys. Rev. Lett. **115**, 266802 (2015).
- 60 F. B. Anders, Phys. Rev. Lett. **101**, 066804 (2008).
- 61 F. Heidrich-Meisner, A. Feiguin, and E. Dagotto, Phys. Rev. B **79**, 235336 (2009).
- 62 X. Zheng, J. Jin, S. Welack, M. Luo, and Y. Yan, J. Chem. Phys. **130**, 164708 (2009).
- 63 F. Jiang, J. Jin, S. Wang, and Y. Yan, Phys. Rev. B **85**, 245427 (2012).
- 64 X. Zheng, Y. Yan, and M. D. Ventura, Phys. Rev. Lett. **111**, 086601 (2013).
- 65 R. Härtle, G. Cohen, D. Reichman, and A. Millis, Phys. Rev. B **88**, 235426 (2013).
- 66 R. Härtle and A. Millis, Phys. Rev. B **90**, 075409 (2014).
- 67 C. Schinabeck, R. Härtle, and M. Thoss, Phys. Rev. B **94**, 201407(R) (2016).
- 68 G. Cohen and E. Rabani, Phys. Rev. B **84**, 075150 (2011).
- 69 E. Wilner, H. Wang, M. Thoss, and E. Rabani, Phys. Rev. B **92**, 195143 (2015).
- 70 H. Wang and M. Thoss, J. Chem. Phys. **131**, 024114 (2009).
- 71 H. Wang, I. Pshenichnyuk, R. Härtle, and M. Thoss, J. Chem. Phys. **135**, 244506 (2011).
- 72 H. Wang and M. Thoss, J. Chem. Phys. **138**, 134704 (2013).
- 73 H. Wang and M. Thoss, J. Chem. Phys. **145**, 164105 (2016).
- 74 H. Wang and M. Thoss, J. Phys. Chem. A **117**, 7431 (2013).
- 75 A. Hewson, *The Kondo Problem to Heavy Fermions* (Cambridge Press, Cambridge UK, 1993).
- 76 W. van der Wiel, S. Franceschi, T. Fujisawa, J. Elzerman, S. Tarucha, and L. Kouwenhoven, Science **289**, 2105 (2000).

- 77 K. Wilson, *Rev. Mod. Phys.* **47**, 773 (1975).
- 78 P. Anderson, *Phys. Rev.* **124**, 41 (1961).
- 79 J. Eckel, F. Heidrich-Meisner, S. Jakobs, M. Thorwart, M. Pletyukhov, and R. Egger, *New. J. Phys.* **12**, 043042 (2010).
- 80 C. Benesch, M. Rode, M. Cizek, R. Härtle, O. Rubio-Pons, M. Thoss, and A. Sobolewski, *J. Phys. Chem. C* **112**, 9880 (2008).
- 81 H. Wang and M. Thoss, *J. Chem. Phys.* **124**(3), 034114 (2006).
- 82 M. Thoss, H. Wang, and W. H. Miller, *J. Chem. Phys.* **115**(7), 2991 (2001).
- 83 H. Wang, M. Thoss, and W. H. Miller, *J. Chem. Phys.* **115**(7), 2979 (2001).
- 84 H. Wang and M. Thoss, *J. Chem. Phys.* **119**(3), 1289 (2003).
- 85 A. Goldberg and B. W. Shore, *J. Phys. B* **11**, 3339 (1978).
- 86 R. Kosloff and D. Kosloff, *J. Comput. Phys.* **63**, 363 (1986).
- 87 D. Neuhauser and M. Baer, *J. Chem. Phys.* **90**, 4351 (1989).
- 88 T. Seideman and W. H. Miller, *J. Chem. Phys.* **96**, 4412 (1991).
- 89 H. Wang and M. Thoss, *Chem. Phys.* **370**, 78 (2010).
- 90 H. Wang, *J. Phys. Chem. A* **119**, 7951 (2015).
- 91 J. Frenkel, *Wave Mechanics* (Clarendon Press, Oxford, 1934).
- 92 H.-D. Meyer, U. Manthe, and L. S. Cederbaum, *Chem. Phys. Lett.* **165**(1), 73 (1990).
- 93 U. Manthe, H.-D. Meyer, and L. S. Cederbaum, *J. Chem. Phys.* **97**, 3199 (1992).
- 94 M. H. Beck, A. Jäckle, G. A. Worth, and H. -D. Meyer, *Phys. Rep.* **324**(1), 1 (2000).
- 95 H.-D. Meyer and G. A. Worth, *Theor. Chem. Acc.* **109**, 251 (2003).
- 96 H.-D. Meyer, F. Gatti, and G. Worth, *Multidimensional Quantum Dynamics: MCTDH Theory and Applications* (Wiley-VCH, Weinheim, 2009).
- 97 M. Thoss, I. Kondov, and H. Wang, *Chem. Phys.* **304**, 169 (2004).
- 98 M. Thoss and H. Wang, *Chem. Phys.* **322**(1-2), 210 (2006).
- 99 H. Wang and M. Thoss, *J. Phys. Chem. A* **111**, 10369 (2007).
- 100 I. R. Craig, M. Thoss, and H. Wang, *J. Chem. Phys.* **127**, 144503 (2007).
- 101 K. A. Velizhanin, H. Wang, and M. Thoss, *Chem. Phys. Lett.* **460**, 325 (2008).
- 102 H. Wang, D. Skinner, and M. Thoss, *J. Chem. Phys.* **125**, 174502 (2006).
- 103 U. Manthe, *J. Chem. Phys.* **128**, 164116 (2008).
- 104 U. Manthe, *J. Chem. Phys.* **130**, 054109 (2009).

- ¹⁰⁵ H. Wang and M. Thoss, *J. Chem. Phys.* **146**, 124112 (2017).
- ¹⁰⁶ O. E. Alon, A. I. Streltsov, and L. S. Cederbaum, *Phys. Rev. A* **77**, 033613 (2008).
- ¹⁰⁷ T. Kato and H. Kono, *Chem. Phys. Lett.* **392**, 533 (2004).
- ¹⁰⁸ J. Caillat, J. Zanghellini, M. Kitzler, O. Koch, W. Kreuzer, and A. Scrinzi, *Phys. Rev. A* **71**, 012712 (2005).
- ¹⁰⁹ M. Nest, T. Klamroth, and P. Saalfrank, *J. Chem. Phys.* **122**, 124102 (2005).
- ¹¹⁰ U. Manthe and T. Weike, *J. Chem. Phys.* **146**, 064117 (2017).
- ¹¹¹ K. Balzer, Z. Li, O. Vendrell, and M. Eckstein, *Phys. Rev. B* **91**, 2015 (045136).
- ¹¹² A. Oguri, *J. Phys. Soc. Jpn.* **74**, 110 (2005).

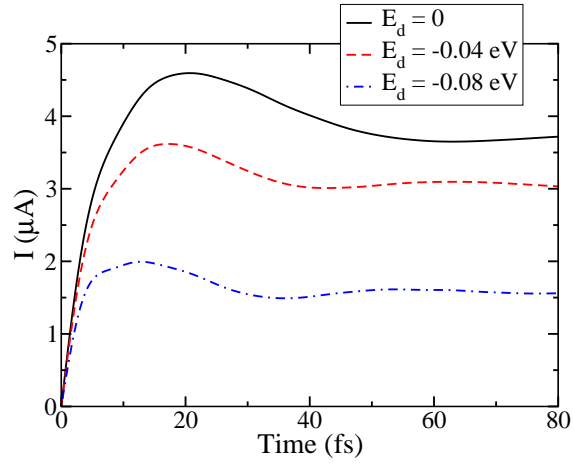


FIG. 1: Time-dependent current for bias voltage $V = 0.1V$ and zero temperature. The square model of Eq. (2.3) is used. The parameters are: $\delta = 4 \times 10^{-4}$ eV, $\Gamma_{L/R} = 0.02$ eV, $E_c = 0.4$ eV, $E_f = 0$, and maintaining $E_d = -U_d/2$.

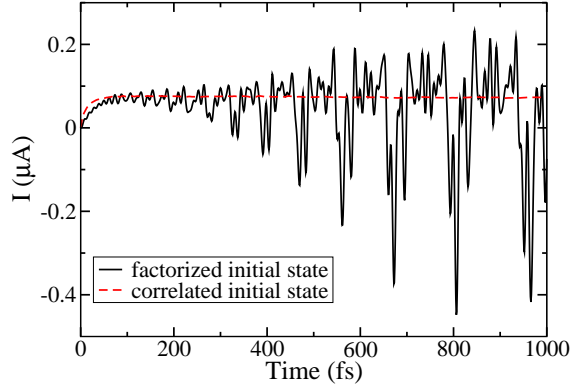


FIG. 2: Time-dependent current for bias voltage $V = 0.001V$ and zero temperature. The square model of Eq. (2.3) is used, where 216 discrete states per lead are employed in the logarithmic discretization, Eq. (3.4), with $\Lambda = 1.175$. The parameters are the same as in Fig. 1 except $E_d = U_d = 0$. For the correlated initial state a fictitious temperature of $T = 2.5K$ was used in the imaginary-time relaxation calculation.

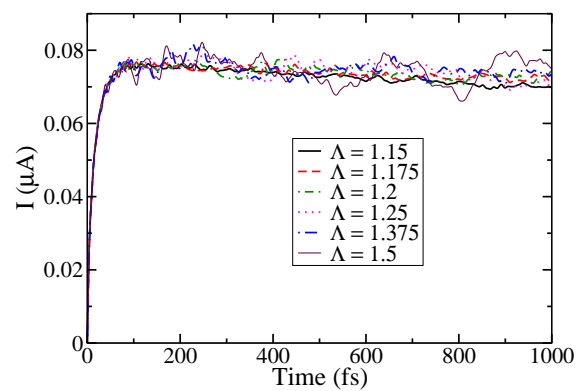


FIG. 3: Time-dependent current versus parameter Λ in Eq. (3.4). The parameters are the same as in Fig. 2, where a correlated initial state is prepared using imaginary time ML-MCTDH propagation with a fictitious temperature of $T = 2.5K$.

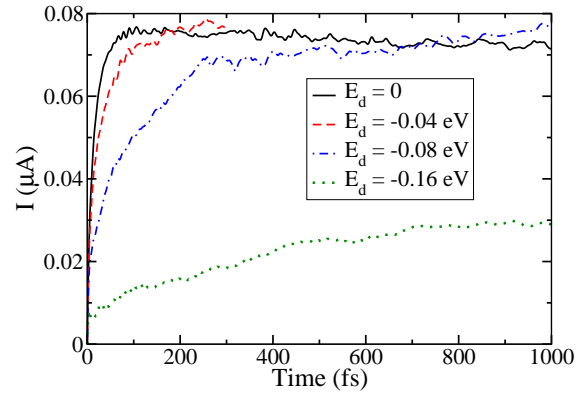
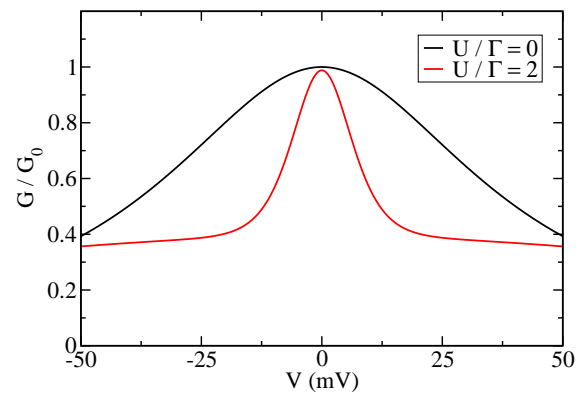


FIG. 4: Time-dependent current for bias voltage $V = 0.001V$ and zero temperature. The square model of Eq. (2.3) is used. The parameters are the same as in Fig. 3, while keeping $E_d = -U_d/2$.

(a)



(b)

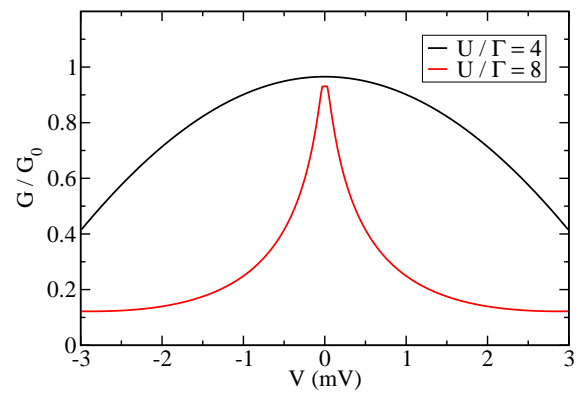


FIG. 5: Conductance versus bias voltage. The square model of Eq. (2.3) is used. The parameters are the same as in Fig. 3, while keeping $E_d = -U_d/2$.